INTERFACE FOCUS

royalsocietypublishing.org/journal/rsfs

Research

Cite this article: Hammerberg AG, Kramer PA. 2021 Consistent inconsistencies in braking: a spatial analysis. *Interface Focus* **11**: 20200058.
https://doi.org/10.1098/rsfs.2020.0058

Accepted: 21 June 2021

One contribution of 12 to a theme issue 'Biological anthroengineering'.

Subject Areas:
biomechanics

Keywords:
anthroengineering, spatial statistics, human movement, centre of pressure

Author for correspondence:
Alexandra G. Hammerberg
e-mail: aghammer@uw.edu

Electronic supplementary material is available online at https://doi.org/10.6084/m9.figshare.c.5486293.

THE ROYAL SOCIETY PUBLISHING

Consistent inconsistencies in braking: a spatial analysis

Alexandra G. Hammerberg and Patricia Ann Kramer

Primate Evolutionary Biomechanics Laboratory, University of Washington, Seattle, WA 98195-3100, USA

AGH, 0000-0002-1219-5007; PAK, 0000-0002-6435-9130

The dynamic system that is the bipedal body in motion is of interest to engineers, clinicians and biological anthropologists alike. Spatial statistics is more familiar to public health researchers as a way of analysing disease clustering and spread; nonetheless, this is a practical approach to the two-dimensional topography of the foot. We quantified the clustering of the centre of pressure (CoP) on the foot for peak braking and propulsive vertical ground reaction forces (GRFs) over multiple, contiguous steps to assess the consistency of the location of peak forces on the foot during walking. The vertical GRFs of 11 participants were collected continuously via a wireless insole system (MoticonReGo AG) across various experimental conditions. We hypothesized that CoPs would cluster in the hindfoot for braking and forefoot for propulsion, and that braking would demonstrate more consistent clustering than propulsion. Contrary to our hypotheses, we found that CoPs during braking are inconsistent in their location, and CoPs during propulsion are more consistent and clustered across all participants and all trials. These results add to our understanding of the applied forces on the foot so that we can better predict fatigue failures and better understand the mechanisms that shaped the modern bipedal form.

1. Introduction

The portion of the human foot that is in contact with the ground (the sole of the foot) during bipedal walking is the primary point of balance for the body above it, allowing for movement through a variable environment. Yet, the sole of the foot is not a large surface area compared to the rest of the body. During walking, two maxima in ground reaction force (GRF) occur in each step, one associated with braking and one with propulsion (e.g. [1,2]). While the magnitude of these forces has received considerable attention (e.g. [3,4]), the location of the centre of pressure (CoP)—the resultant location of all forces applied to the sole—has been less investigated [5,6]. GRFs are a fundamental variable in most biomechanical analyses (e.g. [7–10]), often used to determine joint moments (e.g. [10]), but the location where a force is applied is as critical as its magnitude in determining moments, which are defined as the application of a force through a distance [11]. Consequently, knowing the location of the CoP of the GRF, because it determines the distance, is important. Further, gait (e.g. velocity) and substrate (e.g. gradient; treadmill versus over ground) characteristics are known to affect force magnitude (e.g. [7,10,12–14]), but their effect, or lack thereof, on CoP location is unknown.

In this study, we determine the CoP location of the peak braking and propulsion vertical GRFs for several walking conditions and consider the degree to which the CoP locations are clustered across multiple contiguous steps. Highly clustered CoP locations indicate that biomechanical analyses might draw on data derived from a few steps, as most steps are consistent with others. Less clustered CoP locations point to the need for more steps to be evaluated, as the CoP of any particular step could vary substantially from another. We hypothesize that the CoP location of the peak braking GRF is consistently located in the hindfoot while that of peak propulsion is in the medial forefoot (about which we provide more detail below).

1.1. Forces matter for many reasons

The biomechanics of the human foot is relevant to researchers in many fields, including human evolutionary anthropology, biomechanical engineering and medicine. The derived bipedalism of hominins is of particular interest to evolutionary anthropology because bipedalism is unique among primates and this shift in locomotor behaviour required morphological changes to the musculoskeletal system to accommodate the change in magnitudes and locations of the application of the forces produced during locomotion (e.g. [15,16]). Understanding the biomechanics of hominin mobility is key to understanding human evolution, and the derived morphology of the modern human foot is one of the more substantial differences between the anatomy of modern humans and extant and extinct non-human primates. This morphological difference is associated with bipedalism (e.g. [15,17]). For example, it has been postulated that habitual bipedalism required the development of the non-divergent hallux and a medial arch of the human foot (e.g. [18]). These human features work in tandem to create a relatively stiff lever, a morphological adjustment to the musculoskeletal system directly connected to the locations of the applied forces (e.g. [19–21]). The locations and magnitudes of applied forces on bony systems have, therefore, evolutionary and ontogenetic impacts on the musculoskeletal system at the level of both short (developmental change in the lifetime of an individual) and long time scales (evolutionary change over millions of years) (e.g. [17,19–21]). Through better understanding the locations of peak GRFs during bipedal walking, we gain insight into not only the function of the foot, but also the form as it has developed over these multiple time scales (e.g. [18,22]).

The biomechanics of human movement and its consequences for the musculoskeletal system have also been of long-term interest to engineers. For instance, Wolff's Law was inspired by the observations of structural engineer Karl Culmann of human femoral sections produced by his anatomist colleague Hermann von Meyer [23]. Today the biomechanics of human movement is a key component of engineering, from ergonomics (e.g. [24]) to medical device development (e.g. [25]) to product design (e.g. [26]). All musculoskeletal elements are impacted by the magnitude and CoP locations of the GRFs that travel through the foot during the gait cycle (e.g. [2,3,27]). For instance, the locations and magnitudes of GRFs determine joint moments throughout the weight-bearing system and joint moments influence muscle forces (e.g. [3,27–29]). Slight adjustments to the action of the foot during the gait cycle result in broad changes to the rest of the body in motion (e.g. [3,28]). For instance, bone is not a standard engineered material like steel or reinforced concrete. Bone is strain sensitive—it grows or resorbs due to loads imposed on it—and strains derive from both force magnitude and application location (see e.g. Wolff's original 1867 paper, reprinted 2010 [30,31]). Bone remodels based on the magnitudes and locations of applied forces, whether they are internal muscular forces or external applied forces. Conflicting evidence for the level of this sensitivity, however, and whether bone remodels to prevent fatigue failure (chronic, lower-magnitude loading) or more acute failure (higher-magnitude, but more infrequent loading) muddles our current understanding of skeletal morphology [32,33]. Highly precise loads, as mentioned above, may change skeletal morphology in ways that differ from changes that result from more diffuse loading patterns. Disentangling these threads requires information about loading location because a load with an application area that is concentrated is locally higher than that with similar magnitude spread over a greater application area.

The foot is also clinically relevant. In any system, high forces that repeatedly occur in the same location lead to localized fatigue failures that can be catastrophic to the function of the system (e.g. [34]). In the human body, walking constitutes cyclic loading of the dynamic bipedal system (e.g. [35]). Precision in the location of forces on the foot during the gait cycle, in conjunction with extreme force magnitudes, may lead to localized failures of the system, i.e. acute damage to the soft tissue or bone from a traumatic event. Cyclic loading at non-peak magnitudes, or in more diffuse locations on the foot, can also result in a loss of mobility due to pain or injury over longer periods of time (e.g. [35]), even though the musculoskeletal system has, presumably, developed in response to these chronic loads. Nonetheless, foot structure is variable (e.g. arch height [36]; midtarsal break [37]; compliance [38]), with potential impacts on the location of the CoP (e.g. [5,6]). Consequently, in order to understand the evolutionary pressures associated with bipedalism, the biomechanical consequences of human mobility and the effectiveness of medical treatments, understanding the GRFs and associated CoPs of movement over variable terrains, gradients, burden regimes and speeds is necessary.

1.2. Ground reaction forces

The work described herein extends the work of previous walking studies (e.g. [13,39–44]) to gather GRF data from the foot–surface interaction outside of the confines of the laboratory across multiple, contiguous steps. GRFs reflect the interaction between the foot and the substrate during the stance phase of gait, and two peaks in the vertical component of the GRF are typical in walking (figure 1). The body slows in early stance (the braking period) producing, on occasion, an early transient force spike, then a GRF peak, passes above the stance foot in midstance with a decrease in the GRF, and accelerates in late stance (the propulsive period) producing another GRF peak. In healthy adults, the vertical force peaks coincide with peaks in the anteroposterior direction that reflect braking and propulsion, but this congruence does not always manifest in children or people with pathologic gait (e.g. [45–47]). GRF magnitude varies with factors that include, but are not limited to, mass of the body in motion, velocity of travel (e.g. [27]), system pathology (e.g. [1]), burdens carried (e.g. [48]) and surface type (e.g. [12]).

While the variation in GRF magnitude is well known, the location of the CoP at these peak vertical GRFs, however, is less well established. The heel is typically the first anatomical feature to strike the ground and the toes are the last to leave during a step, but the CoP location when peak vertical (braking and propulsion) force occurs and its consistency of placement is less explored (e.g. [49]). Grundy *et al*. [5] found that the peak braking vertical GRF occurs when most of the foot is already in contact with the ground, but they were limited by the force plate technology of the time and did not examine in detail the consistency of this placement or whether it varies based on velocity, substrate or gradient. Croft & Bertram [6] recently examined the foot–ground interaction during bipedal walking through the lens of bipedal optimization, noting that the CoP, as it travels along the foot, plays

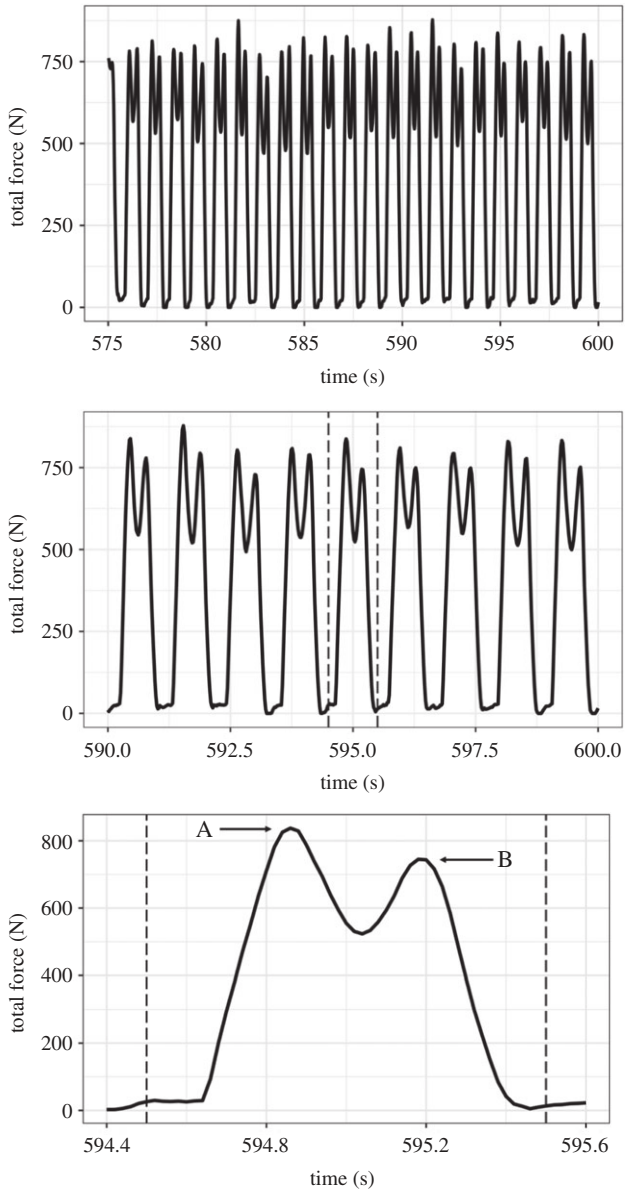

Figure 1. Vertical GRF for left foot. Isolated individual left foot steps for one participant (body weight at stance = 812 N) during hallway walking at self-selected velocity. The vertical force curve for a single foot over the course of the gait cycle. 'A' denotes peak vertical force at braking and 'B' denotes peak vertical force at propulsion. Dashed lines isolate a single interaction between the foot and the ground, with panels progressively displaying a shorter time frame.

an integral role in predicting the overall dynamics of the system. The CoP at peak GRF indicates where the resultant of the contact forces between the foot and substrate act on the foot during a gait cycle. The CoP at peak GRF over multiple gait cycles describes the nature of the cyclic loading of the musculoskeletal system. As with any dynamic system, repeated loading patterns play an important part in system design to ensure durability, i.e. these systems are designed for fatigue loading, as discussed above. It is crucial, therefore, that we understand where the CoPs at peak forces occur on the foot, not just over one loading cycle, but over many loading cycles, to fully grasp the system dynamics as a whole and what it implies for human bipedal mobility.

1.3. Spatial statistics

The spatial nature of CoP measurements requires a different methodology than one would use for GRF magnitude data. Spatial statistics is an analytical method for quantifying the distribution of data over a physical region. Most often used in epidemiology or geographical analyses to examine disease events (e.g. [50–52]), spatial statistics has diverse applications (e.g. tree clusters [53], mineral contents [54], neuron distribution in the brain [55]). Spatial statistics methods are also found in a variety of engineering disciplines (e.g. mechanical engineering [56], geological engineering [57], electrical engineering [58], environmental engineering [59,60] and petroleum engineering [61]). Applying this methodology to examine point positions of CoP on the sole of the foot is an extension of these problems where we treat the sole of the foot as geography at a smaller length scale.

Pedobarography is the study of the pressure pattern of the sole of the foot during stance or movement (e.g. [62–65], etc.). The pressure distribution of the GRF drives the biomechanics of the entire body and so has been used to assess the biomechanics of gait (e.g. [21]). Pedobarographic data are also used by clinicians to determine which section of the foot is in contact with the ground in order to assess pathology of movement or investigate the impact of those pathologies on foot mechanics (e.g. [62,64]). A variety of statistical analysis methodologies have been applied to address the spatio-temporal nature of pedobarographic data, ranging from image analysis techniques (e.g. [63]) to statistical parametric mapping (e.g. [66]) in addition to more simplified analyses of the magnitude of pressures (e.g. [67]).

This project developed from our interest in the consistency of the location of CoPs across many loading cycles and conditions (e.g. speeds, terrains and gradients). Modern humans do not move only at a single speed along flat surfaces, and we wanted to capture any potential for variability along different terrains and at different speeds. Most pedobarographic work relies on pressure pads or force plates set into the floor to capture participant data (e.g. [64,65], etc.). This approach restricts researchers to collecting a few steps over the course of several trials, which increases the potential for variability across trials. By using wireless, pressure-sensing insoles (Moticon ReGo, Munich, Germany), we were able to collect CoP data over multiple, contiguous steps for all participants and all trials both within and outside of the confines of the laboratory. We used Ripley's clustering *K*-function [68,69] to quantify the consistency of CoP location during the peak braking and peak propulsive vertical GRFs. To our knowledge, this work is the first to apply spatial clustering analyses to look at the consistency of CoP on the foot during multiple, contiguous gait cycles across different terrains and at different speeds.

1.4. Hypotheses

Feet are the primary point of contact with the environment and subject to the cyclic forces of locomotion from heel strike to toe off. The applied loads to the hindfoot react directly into the tibia through joint (tibiotalar) contact, forming a stable, compressive column, while loads applied to the forefoot (e.g. loads applied under the metatarsal heads) rely on the mid- and forefoot (which form the longitudinal arch) to act as a rigid, cantilevered beam. Given that this beam is composed of numerous bones linked by ligaments and the action of muscles, some flexibility in the arch is possible. Based on these mechanical considerations, we predict that the location of the CoP will be consistently clustered in the hindfoot for the braking peak and consistently in the

Table 1. Participant data, including average self-selected velocities for the overground walking trials.

participant	age	mass (kg)	neutral standing force (N)	insole size	arch index	hallway (m s^{-1})	downhill (m s^{-1})	uphill (m s^{-1})
X1	26	70.2	868	8/9	0.244	1.43	1.52	1.51
X3	29	86.4	819	9.5/10.5	0.182	1.24	1.5	1.56
X4	20	120	1176	11/12	0.424	1.29	1.49	1.36
X5	21	70.7	692.9	8/9	0.235	1.2	1.43	1.52
X6	28	52	509.6	6.5/7.5	0.252	1.15	1.32	1.46
X7	42	86	842.8	9.5/10.5	0.249	1.24	1.41	1.39
X9	29	55	539	6.5/7.5	0.128	1.12	1.28	1.34
X10	20	48.9	479.2	6.5/7.5	0.089	1.11	1.5	1.33
X11	32	72.9	714.4	8/9	0.162	1.15	1.34	1.24
X12	21	54.6	535.1	6.5/7.5	0.159	1.24	1.39	1.47
X13	32	66.5	651.7	8/9	0.349	1.23	1.47	1.52

forefoot for the propulsion peak across all conditions and all participants. We also predict that there will be no difference in degree of clustering, as assessed by Ripley's *K*-function, of CoP points between braking and propulsion within trials.

2. Methods

2.1. Participants

The data were collected from a convenience sample of 11 participants (six females and five males) ages 20–42 years (table 1), who were without gait pathology or injury to their lower limbs within the last 2 years. We measured their mass (kg) with a standard scale and calculated a neutral stance force, which was equal to the sum of the force exerted on both insoles while the participant stood quietly. Arch index (AI) was calculated as the ratio of midfoot area to total foot area during quiet standing [70] from footprints for each participant obtained from a pressure mat (RSscan International, Olen, Belgium).

2.2. Experimental set-up

Each participant was fitted with a pair of wireless pressure-sensing insoles (Moticon ReGo AG, Munich, Germany) worn in a pair of water socks (Fitkicks™). We used the water socks to limit the effect of variability in shoe sole stiffness and obtain a condition as close to unshod as possible. Thirteen force sensors are distributed across the insole surface and were set to collect data at 50 Hz (i.e. every 0.02 s). Each sensor recorded a force value at each time point. The total force summed across the sensors and the CoP X (medial–lateral) and Y (posterior–anterior) coordinates were also determined at each time point. The insoles were calibrated through the Moticon ReGo AG software and checked by the researchers to ensure tare had been reached before being donned by the participants. Each participant's mass was recorded using a tared laboratory scale and the insole force reading was compared to the scale reading. The insole's CoP sensitivity falls within ±20 mm, according to the company's specifications, and has been validated against a force plate system in prior work [71].

We investigated seven walking conditions. Participants walked on a treadmill at 0.89 m s^{-1} (slow), 1.34 m s^{-1} (moderate) and 1.79 m s^{-1} (fast) for 60 s at each velocity. The order of these treadmill tests was randomized. Participants then walked on the treadmill set to a 10% slope at 0.89 m s^{-1}. Participants also walked at their comfortable pace along a straight, flat, 78.4 m indoor hallway. Lastly, participants walked at a self-selected pace in a straight line on an outdoor sidewalk, downhill and uphill over 70.5 m on an 8.8% slope in dry conditions. Research personnel ensured that the hallway and outside paths were unobstructed during the trials. This project was approved by the University of Washington Institutional Review Board.

2.3. Data acquisition and initial processing

We isolated individual steps for each trial from the total force for the left and right foot of each participant (figure 1) and determined the local force maxima for the braking and propulsive phases of stance from each step using a custom-written MATLAB (MathWorks) program. We removed steps with fewer or more than two peaks as indicative of non-normal (e.g. 'stumble') steps. In total, 6711 steps were analysed across all participants and all trials.

We standardized the X and Y coordinates of the CoP to account for insole size differences between participants by multiplying by the insole scaling factor provided by manufacturer Moticon ReGo AG. This normalized all participants to the size 8/9 insole coordinate system. In our initial exploration of the data, we found no indication of left–right asymmetries for any of our participants; therefore, the signs on the X coordinates were flipped for the right foot to match the left foot coordinate world. We compared the position of the CoP during the braking and propulsive phases between conditions and between individuals in each condition. We calculated the individual velocities for each participant's hallway, downhill and uphill trials from time and distance travelled.

To ensure that the disparity in the number of data points between trials did not impact our analysis, we normalized the number of steps in each trial. Slow treadmill walking had 572 steps total, the fewest across our trials, so we took a random sample without replacement of 572 steps from each of our trials.

2.4. Statistical analysis

Ripley's second-order intensity function, $K(d)$, is a method of quantifying clustering [50,68,69,72] and is derived from Ripley 1987 [69] as:

$$K(d) = \frac{\sum [\text{number of further events within distance } d \text{ of an arbitrary event}]}{\lambda},$$

where λ is the intensity, or average number of points (n), within a unit area.

The formal estimation of the K-function is described mathematically as

$$\hat{K}(d) = \frac{1}{\hat{\lambda}} \sum_{i=1}^{n} \frac{1}{n} \sum_{j \neq i} \text{binary indicator 1 if } d_{ij} \leq d,$$

where d_{ij} is the distance between points i and j.

Ripley's K-function $K(d)$ is dependent on the number of events within a distance d (in metres), or in this case, the number of CoP point occurrences within a certain distance. If the peaks exhibit complete spatial randomness (CSR), i.e. no discernible clustering, $K(d)$ will be approximately equal to πd^2, but if the data are clustered, then we expect $K(d) > \pi d^2$ for small d. From this estimator, we can quantitatively compare clustering at a given d between trials as well as between braking and propulsion peaks within a trial to determine consistency of location of CoP points.

2.5. Defining significance in spatial clustering analysis

We used Monte Carlo sampling to establish a baseline variability for our $K(d)$ estimation by generating 100 simulations of CSR sets of 572 points. CSR points were generated within the insole polygon boundary using the R packages 'lattice' [73] and 'spatstat' [72]. These generated points form the 95% pointwise simulation envelopes, or 'acceptance envelope'. We used these CSR points as our null $K(d)$ to assess clustering for braking and propulsion in each trial. A high degree of clustering, i.e. a $K(d)$ value falling above our 95% pointwise acceptance envelopes for a given d, indicates consistent CoP placement recurring over multiple gait cycles. Values that fall within the acceptance envelope for a given d are considered non-significant; values that fall outside of the acceptance envelope are considered significant [72].

In order to compare the CoP point patterns between trials, we adapted the methodology typically used to compare the spatial location of case versus control points in public health and epidemiology studies (e.g. [50]), which applies binary marks (e.g. 1 = case, 0 = control) to each set of points. This enables direct assessment of the clustering in one group of points compared to the other. In our adaptation, we performed pairwise comparisons for all trials; essentially labelling one trial as 'cases' and the other as 'controls' in each analysis. We analysed between all trials for CoP at peak braking and between all trials for CoP at peak propulsion. We also compared the clustering of peak braking and propulsion CoP points within each trial.

We used the Monte Carlo method for generating our acceptance envelope in each pairwise comparison by randomly relabelling the points in the two trials over the course of 100 simulations per pairwise comparison [72]. For example, in the pairwise comparison of slow versus moderate treadmill walking, each CoP point during braking was randomly relabelled as either slow or moderate to establish the Monte Carlo envelope boundaries. If the difference in $K(d)$ between the two trials was outside of that envelope, we determine that the level of clustering between the two trials is different.

Since all participants performed all trials, our covariates were limited to the differences in each trial's velocity, surface type and gradient. As described above, we define statistical significance for this analysis as values outside of the simulated Monte Carlo acceptance envelopes, as this is the relevant statistical test for this methodology [72]. For all analyses, values that fall within the acceptance envelope are considered non-significant, values that fall outside of the acceptance envelope are considered significant. For further discussion of Ripley's K-function as well as Monte Carlo acceptance envelopes for determining significance, refer to Baddeley *et al*. [72].

Note that the $K(d)$ values of trials with CoP points that are similarly distributed will be approximately equal across all values of d, and the difference in $K(d)$ will fall within the acceptance envelope; i.e. there is no significant difference (as defined above) in $K(d)$ values [72]. For trials where the CoP point distribution is significantly dissimilar (i.e. one trial is very clustered with a high $K(d)$ and the other trial has a more diffuse point distribution), the difference in $K(d)$ will fall outside of the acceptance envelope. In the case of a large difference in $K(d)$ between compared trials, when d increases beyond the point range of the more clustered trial, $K(d)$ falls to zero (because there are no CoP points remaining outside d for that trial), and the difference in $K(d)$ between trials is the value of K at distance d of the less clustered trial. The difference in $K(d)$ between trials, then, is significantly different if it is outside the acceptance envelope in either the positive or negative direction [72].

Using the foot segmentation described below (forefoot, midfoot, hindfoot), we calculated the percentage of CoP points in each region during peak braking GRF and peak propulsive GRF for each trial by dividing the number of CoP points in each region by the total steps in each trial. To assess whether or not a relationship exists between the number of points in a foot region and participant characteristic (e.g. AI), we fit generalized linear models and we accounted for the hierarchical groupings of trial and participant in all analyses.

We used an assortment of RStudio packages in our analyses. These included: 'lattice' [73], 'sp' [74], 'splancs' [75], 'spatstat' [72], 'lme4' [76] and 'uwIntroStats' [77].

2.6. Sample area

The boundaries (edges) of the sample area were provided as coordinate points for a size 8/9 US (42/43 UK) insole by Moticon ReGo AG. These points were then converted into a spatial polygon and the insole data points were generated within this boundary using the R packages 'lattice' [73] and 'spatstat' [72]. We determined that, based on the distribution of points across all trials and the lack of points outside of the sample area, it was not necessary to account for edge effects. None of the CoP points for braking or propulsion for any of the trials were close enough to the edge of the insole to warrant concern regarding edge effects in the analyses and each insole was fitted to entirely contain the participant's foot.

We partitioned the insole into hindfoot, midfoot and forefoot based on anatomical landmarks. The hindfoot consists of the calcaneus and talus from the posterior heel to the anterior calcaneocuboid joint, which is approximately 38% of the total length of the foot. The midfoot consists of the other tarsals, assessed medially from the navicular tuberosity to the base of the first metatarsal and laterally from the calcaneocuboid junction to the fifth metatarsal tubercle, which is approximately 10% of the total length of the foot. The forefoot consists of the metatarsal and phalangeal systems, medially from the base of the first metatarsal, laterally from the tuberosity of the fifth metatarsal, to the distal phalanges, which is approximately 52% of the total length of the foot. We obtained the proportions of total foot length in each part of the foot by measuring the distances between palpable landmarks. We then applied these proportions for all subjects.

3. Results

Based on the $K(d)$ estimation, CoP points during peak braking and peak propulsion for each trial display clustering relative to the simulated CSR. The difference between the estimated $K(d)$ values for braking and propulsion lies outside of the Monte Carlo acceptance envelope for all trials for

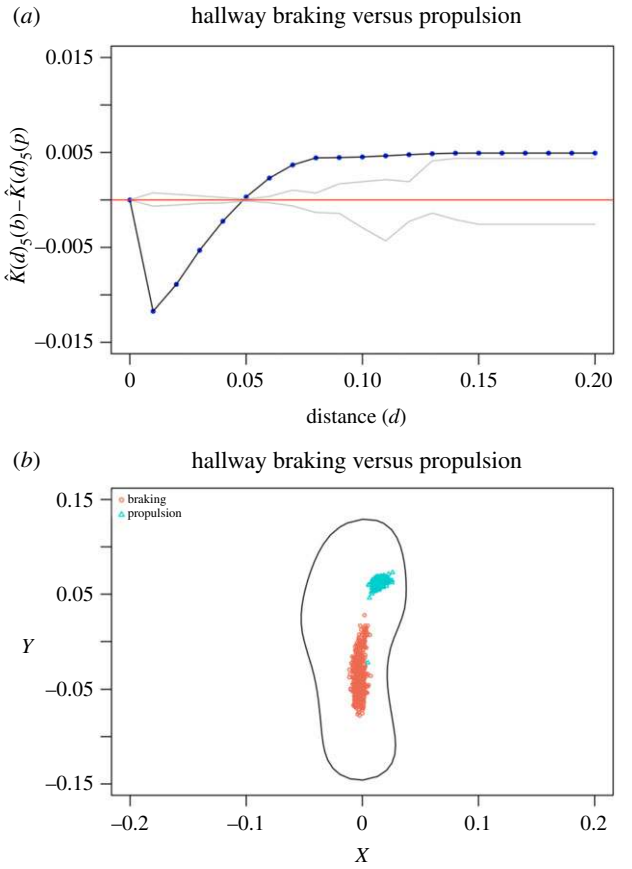

Figure 2. *K*-function estimation for hallway braking compared to propulsion. The solid black line with blue points in panel (*a*) shows the difference in $K(d)$ clustering values between braking CoP points and propulsion CoP points at each tested distance (d, metres). The red line represents no calculable difference in $K(d)$ values, and the grey lines denote the Monte Carlo acceptance envelope if there was no significant difference. There is significantly more clustering in CoP points during propulsion than braking ($K(d)$ propulsion > $K(d)$ braking), so the black line falls outside of the acceptance envelope for distances within the insole area. Panel (*b*) shows the CoP points for braking (red) and propulsion (teal) for all participants during the hallway walking trial.

$d \leq 0.2$ m. The estimated *K*-value for propulsion is greater than the estimated *K*-value for braking for all trials, meaning that propulsion peaks are more tightly clustered than braking peaks. The $K(d)$ clustering comparison between $K(d)$ of braking and $K(d)$ of propulsion for the hallway walking trial is shown in figure 2 as an example of these results. The full graphical results of our clustering analysis for each trial are included in the electronic supplementary material. A difference in $K(d)$ (indicated with blue circles) outside the acceptance envelope (indicated by the grey lines in figure 2) indicates significant clustering. Overall, there are also more pairwise differences in clustering during braking than there are for propulsion.

Table 2 shows the percentage of CoP points in each region of the foot at peak braking GRF and peak propulsive GRF across all participants and all steps. The CoP at peak braking GRF was located in the hindfoot for all trials except downhill walking. Uphill walking, in contrast, demonstrated the most consistent CoP location during braking. The CoP points at peak propulsive GRF were consistently located in the forefoot for all trials. Across all steps for all trials and all participants, less than 0.2% of CoP points at peak propulsive GRF were located elsewhere on the foot. Our results indicate that braking is a less consistent mechanism than propulsion. On the one hand, CoP points at peak braking, while clustered for all trials, are in the hindfoot only 47.4% of the time (figure 3). CoP at peak propulsion, on the other hand, occurs in the forefoot 99.9% of the time across all trials (figure 3). Analysing these results by individual reveals the same pattern (figure 4). Although participants do vary somewhat in the location of their CoP, we found no significant effect of AI or other individual-specific characteristic, so those analyses are not shown.

Table 2. Percentage of CoP points located in each region (fore, mid or hind) of the foot during peak braking GRF and peak propulsive GRF for each trial across all participants. The highest percentage values for braking and propulsion for each trial are indicated in bold.

	% of CoP points at braking	% of CoP points at propulsion
slow treadmill		
forefoot	23.2	**99.8**
midfoot	24.4	0
hindfoot	**52.4**	0.2
moderate treadmill		
forefoot	15.1	**100**
midfoot	39.5	0
hindfoot	**45.5**	0
fast treadmill		
forefoot	8.4	**100**
midfoot	44.7	0
hindfoot	**46.9**	0
inclined treadmill		
forefoot	13.9	**99.9**
midfoot	18.3	0
hindfoot	**67.8**	0.1
hallway walking		
forefoot	11.9	**99.8**
midfoot	42.6	0.2
hindfoot	**45.5**	0
downhill walking		
forefoot	46.8	**99.9**
midfoot	**49.7**	0.1
hindfoot	3.5	0
uphill walking		
forefoot	4.5	**99.9**
midfoot	25.3	0.1
hindfoot	**70.2**	0

4. Discussion

Our goal in conducting this research was to quantify the spatial location and consistency of CoP on the foot during peak force application while walking, specifically, during the braking and propulsion components of the gait cycle. To

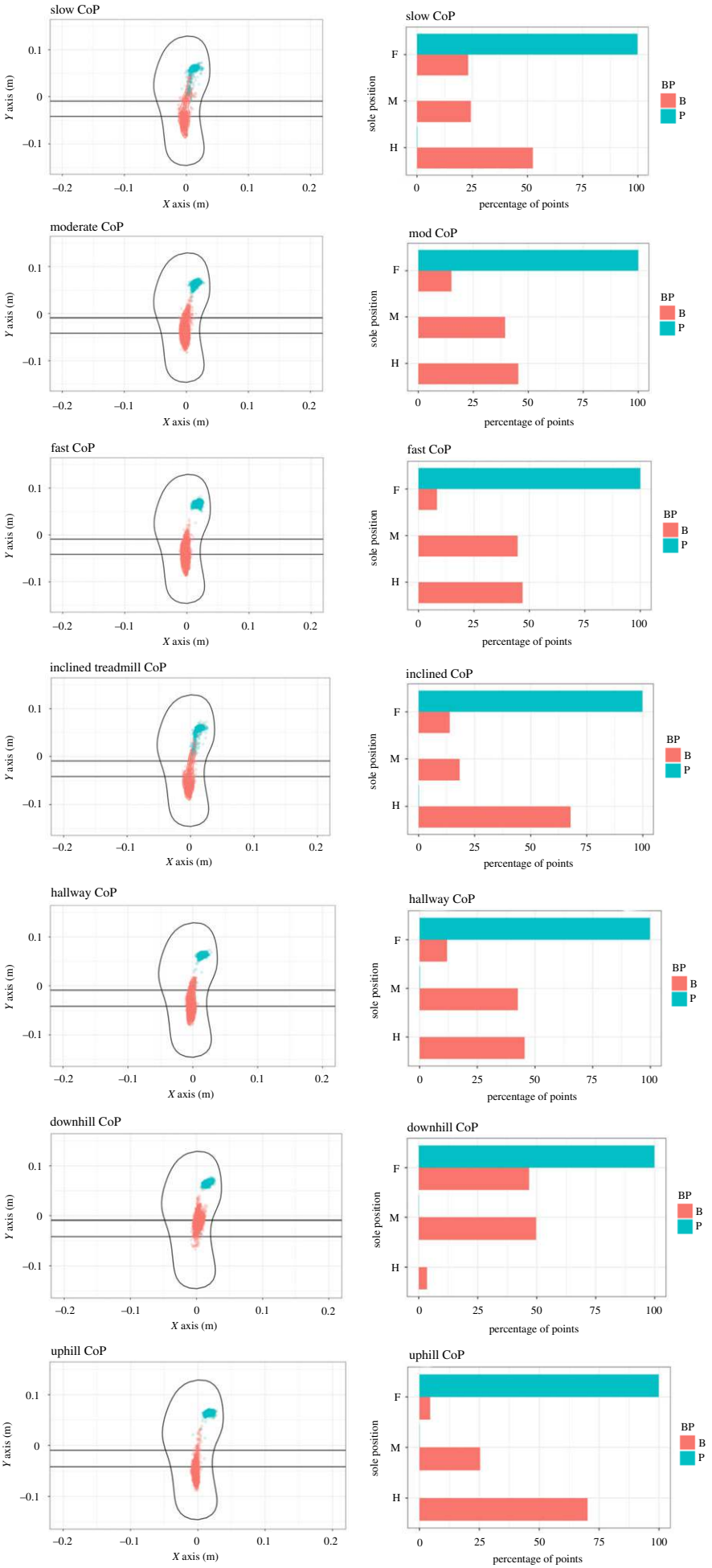

Figure 3. The CoP points and corresponding percentage graphs for each walking trial. Left column: CoP points at peak braking GRF (red) and propulsion GRF (blue) plotted with lines demarcating fore- (F), mid- (M) and hindfoot (H). Right column: the corresponding breakdown of the percentage of points in each region.

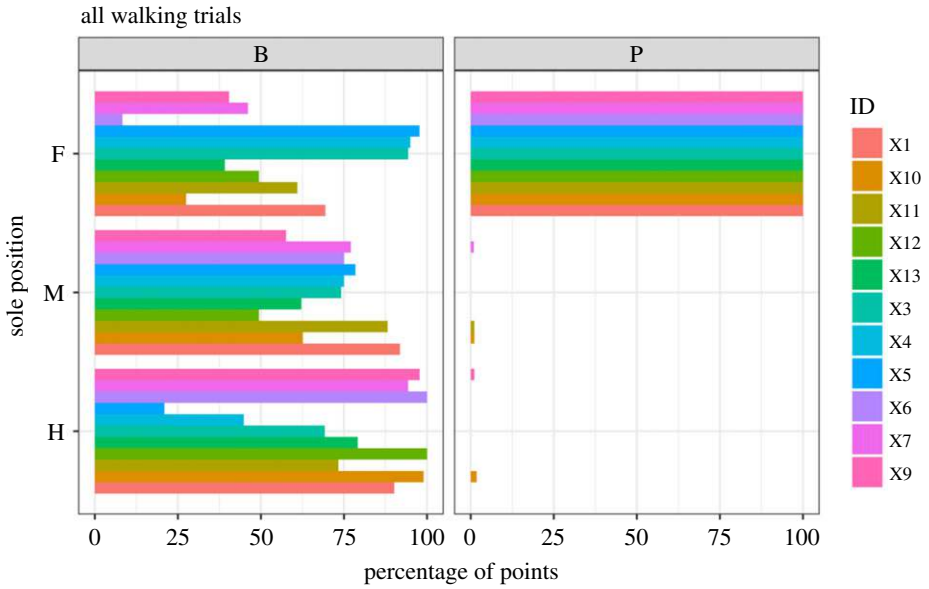

Figure 4. Percentage of CoP points by individual—all walking trials—the percentage of CoP points in each region of the foot (F = forefoot, M = midfoot, H = hindfoot) for all trials, broken down by participant (ID) for braking (column B) and propulsion (column P).

accomplish this, we examined the location of the CoP during peak braking and peak propulsive vertical GRF to determine the clustering pattern of CoP over repeated gait cycles using Ripley's *K*-function. We also quantified the effect of different terrains and walking speeds on CoP location and consistency of placement. Although we could draw initial qualitative conclusions based on our visual assessments of the CoP locations on the foot and consistency both within and across gait cycles, we confirmed quantitatively with Ripley's *K*-function that our qualitative observations were statistically significant. No researchers, to our knowledge, have used clustering analyses from spatial statistical methodologies to assess the consistency of the spatial component of CoP points across multiple, contiguous steps during human walking.

The magnitude and locations of the forces that occur on the foot during habitual movements, e.g. walking, influence the joint moments throughout the musculoskeletal system (e.g. [27]), the potential for fatigue failures at locations of precise, cyclic forces (e.g. [35]), and evolution of human morphology (e.g. [18]). As non-pathological walking along an unobstructed pathway is a consistent, cyclic movement our participants perform daily, we expected the locations of the CoP at peak vertical forces (braking and propulsion) to be relatively consistent across gait cycles. The applied loads to the hindfoot (calcaneus and talus) can react directly into the shank (tibia) through joint (tibiotalar) contact, essentially creating a stable, compressive column. Loads applied to the distal foot rely on the mid- and forefoot to act as a cantilevered beam. Given that the hindfoot load path is much stiffer than that of the forefoot, we expected that the CoP during peak braking would be clustered consistently in the hindfoot, with the potential for shifting proximally towards the midfoot along gradients. We expected CoP at peak propulsion to occur primarily in the forefoot, but, due to the flexibility of the foot, we expected to see CoP spread across the first and second metatarsal heads across gait cycles and participants.

Previous work has examined the locations and magnitudes of peak pressures on the foot during walking (e.g. [5,62,64,65,78–81]), but the consistency of these locations over multiple gait cycles has been less documented. In our initial exploration of the CoP data we noted that, visually, CoP points at peak propulsion were consistently concentrated in the forefoot, with few outliers (figure 3). By contrast, the CoP points at peak braking were diffuse across the foot (figure 3). As this was contrary to our initial expectations, we sought to quantify these qualitative observations. A braking mechanism that results in inconsistent CoP locations across multiple gait cycles may produce variable joint moments and, consequently, variable muscle forces. These variable applied forces to the bone have potential consequences for the bony morphology, as bone responds to applied forces, as well as implications for fatigue failure mechanisms throughout the musculoskeletal system. Evaluating the spatial clustering of CoP points over multiple gait cycles using spatial clustering affirmed our qualitative observations regarding the precision or diffusion of CoP at peak forces on the foot. This, in turn, adds to our understanding of where peak cyclic loads occur on the foot and, therefore, throughout the musculoskeletal system. For example, the role of the lateral midfoot in transferring the braking peak from the substrate to the body may be underappreciated (although variability in pressures exerted by the lateral foot is documented (e.g. [37,38])), which suggests that additional investigation of the lateral foot is warranted. In addition, the lack of consistency in the location of the braking peak has potentially important implications for biomechanical analyses: a small number of steps may be insufficient to capture the full range of lower limb joint moments at the braking peak of the GRF. Although we did not evaluate the shape of the vertical GRF curve, it seems reasonable to extrapolate that the entire first half of stance may not have a consistent pattern of location of the CoP. The location of the CoP of the propulsive vertical GRF peak was remarkably consistent (figure 4). This consistency was apparent even in the participant with the lowest arch (participant X4), potentially indicating that a low AI does not impact the foot's ability to act as a lever during propulsion. Future work should explore the relationship of foot stiffness and its impact on GRF magnitude and location.

The advantage of using Ripley's *K*-function [50,68,69,72] to quantify spatial clustering is that it allowed us the flexibility to

assess the clustering of point data from single trials as well as pairwise point dataset comparisons of clustering. If there was no significant difference in clustering in a pairwise comparison, the difference in $K(d)$ values between the pairs $(K_1(d) - K_0(d))$ would lie within the acceptance envelope. Our primary analysis compared the clustering of CoP points at peak braking GRF to the clustering of CoP points at peak propulsive GRF. We found that the difference in the estimated $K(d)$ value between braking and propulsion lay outside of the acceptance envelope for all trials. The estimated K-value for propulsion is greater than the estimated K-value for braking for all trials, which indicates that propulsion is significantly more clustered than braking for all trials.

We also calculated the percentage of CoP points in each region of the foot (fore, mid, hind) and confirmed that braking is a more variable mechanism. CoP points at peak braking, while clustered for all trials, were in the hindfoot only 47.4% of the time across all trials and in the midfoot 34.9% of the time across all trials (table 2). CoP during peak propulsion occurred in the forefoot 99.9% of the time across all trials. Across all steps for all trials and all participants, less than 0.2% of CoP points during peak propulsive GRF were located elsewhere on the foot. CoP during peak propulsion was tightly clustered around the medial forefoot (e.g. the heads of the first and second metatarsals). This consistency is striking and offers insight into the forces as they are applied to the foot and, subsequently, the body as a dynamic system. Peak braking forces that load the foot, and, therefore, the rest of the body, were more diffuse over the course of many gait cycles, suggesting less potential for fatigue failures to localized areas of the hind- and midfoot over cyclic loading cycles compared to the forefoot and potentially suggesting more variability in load transfer through the leg. With peak vertical GRFs during propulsion falling consistently under the heads of the medial metatarsals, it is unsurprising that pathologies are frequent in this region (e.g. [35]).

We found less variability in CoP location during peak braking when we examined the trial data by participant (figure 4), but there was still more variability in an individual's braking CoP than in an individual's propulsive CoP. The consistency in CoP location during propulsion within individuals was equally pronounced within individuals as across individuals. While the data reveal some structuring by participant (figure 4), we found no predictive metric for this structure. AI was assessed as a covariate in the statistical models, but was not found to be a statistically significant predictor of clustering or location of CoP on the foot during braking or propulsion. While one participant had a low arch (AI = 0.4), no one exhibited a high arch (AI = 0), so this sample is not an ideal one with which to evaluate the potential of AI to influence the location of the CoP. This limitation warrants future exploration of foot morphology (e.g. AI, midtarsal break, medial column divergence) that may influence the location of CoP during peak braking GRF. Future work should also increase the power of these metrics by recruiting participants based on aspects of foot shape. Another limitation was our use of water socks to hold the insole in place against the foot. While we used the socks as a best approximation of barefoot walking in order to gather data across multiple, contiguous steps outside of the laboratory, future work should include comparative, fully barefoot trials along a force plate or pressure pad walkway. Future work also should investigate consistency in peak force location at other times in the gait cycle, such as the point immediately after heelstrike where lower-magnitude, but high-impact, transient forces can occur at initial heel contact [82,83].

Although we did not extend our hypotheses and statistical analyses to specific circumstances, many debates in various fields might potentially be informed by our results, so we note several here. The following examples are not meant to be exhaustive, but rather to be demonstrative. First, discussions of the evolution of the hominin foot have assumed that a pronounced longitudinal arch (e.g. rigid foot) is a requirement for effective propulsion [18,84,85], even if the arch is achieved through facultative muscular contraction [86]. Our results, as mentioned above, indicate that it is possible that a foot with a low arch, which is, presumably, less rigid [18], exhibits the same consistency in CoP location at peak propulsion vertical GRF as a higher arched foot. This suggests that future work should examine the relationship among foot stiffness, GRFs and CoP locations to understand the role of the longitudinal arch in walking.

Another, more clinically applied, area which might be informed by our results is prosthetic design. Insights from considerable efforts to understand such gait-based topics as the importance of weight acceptance (e.g. [87]) and of prosthetic foot stiffness (e.g. [88]) for performance have been used to guide prosthetic design. Nonetheless, lower limb prosthetic design has still failed to reach parity in performance across multiple mobility tasks with that of the natural limb (e.g. [89–91]). Braking and propulsive efforts are known to differ (e.g. [92]) and gait deviations in amputees are common (e.g. [89]). Timmermans *et al*. [93] have demonstrated the usefulness of insoles for determining gait temporal parameters in amputees, but less work has been directed at understanding the role of the variability in CoP location on lower limb biomechanics in amputees. Our work establishes a baseline of expected variability in CoP location in natural limbs that can be used comparatively with prosthesis–ground interactions and that may assist in identifying prosthetic design choices to minimize gait asymmetries between a prosthetic and natural limb.

Finally, while musculoskeletal modelling has become widespread, the inputs frequently include less than a dozen steps even in work designed to understand the impact of variability on the gait metric of interest (e.g. [94,95]). Our results suggest that, while appropriate for the propulsion portion of stance, evaluation of a limited number of steps is not sufficient for the braking portion of stance because the location of the CoP varies even though the magnitude of the GRF may not. A braking mechanism that results in inconsistent CoP locations across multiple gait cycles may produce variable joint moments and, consequently, variable muscle forces. These variable applied forces to the bone have potential consequences for the bony morphology, as bone responds to applied forces, as well as implications for fatigue failure mechanisms throughout the musculoskeletal system. We found these inconsistencies in braking by measuring CoP location over a minimum of 574 steps per individual.

5. Conclusion

The dynamic, bipedal system that is the human body is complex. Movement through the environment is a foundational part of this dynamic system, and humans devote a large

proportion of their energetic resources to this function (e.g. [29,96]). Understanding the dispersion of peak forces on the foot is crucial to understanding bipedal movement in modern humans and informs our understanding of human morphology within the lifetime of an individual and across evolutionary history (e.g. [18,22]). The feet of bipeds are the primary point of contact with the environment and subject to the forces that constitute self-propelled locomotion. The forces associated with the interaction of the human body with the environment through the foot dictate how this movement occurs. While a stable braking mechanism may be helpful, our work indicates that it is not, and therefore does not have to be, a precise mechanism in healthy adults. The consistency of CoP at the peak propulsion suggests that this is the mechanism that is precise, whether due to a requirement for efficiency of forward movement, by necessity for stability or for other reasons. The consistency also implies that the joint moments during peak propulsion are more consistent throughout the weight-bearing system.

Our results regarding the inconsistency of the CoP at peak braking, combined with consistency at peak propulsion, have implications for understanding the evolution of the foot, for its treatment after trauma, and for prosthetic design. Engineered systems see localized fatigue failures when subjected to high-magnitude, precise cyclic loading (e.g. [34]), and the human body is no different (e.g. [35]). The engineering of the foot, in both material composition and form, reflects the need of the system to endure high, contained forces over a small area throughout a human lifespan. By understanding the locations and magnitudes of the forces on the system, we can not only better predict and prevent fatigue failures of the system before they become catastrophic, but also better understand the mechanism that has shaped the bipedal form with which we are familiar today.

Ethics. This project was approved by the University of Washington Institutional Review Board (STUDY00003124/MOD00001410). Participants provided written consent.

Data accessibility. All data used in these analyses are provided as electronic supplementary material [97].

Authors' contributions. Both authors contributed equally to this paper.

Competing interests. The authors have no conflicts of interest to state.

Funding. We received no funding for this study.

Acknowledgments. The authors thank S.K. Benirschke, MD, Jerome Debs Endowment Chair in Orthopaedic Traumatology at the University of Washington, for the ongoing support of this research and for our many conversations about foot form and function. The authors would also like to thank the participants of this study for their time and patience during the protocol. A.G.H. also thanks Dr Jon Wakefield and Dr Marcos Llobera for spatial statistics guidance, and the NSF Graduate Research Fellowship Program for their continued support of her work.

References

1. Perry J. 1992 *Gait analysis: normal and pathological function*. Thorofare, NJ: SLACK Inc. (Second edition: Perry J, Burnfield JM. 2010.)
2. Inman VT. 1966 Human locomotion. *Can. Med. Assoc. J.* **94**(20), 1047–1054. See https://www.ncbi.nlm.nih.gov/pmc/articles/PMC1935424/pdf/canmedaj01164-0022.pdf.
3. Cavagna GA, Margaria R. 1966 Mechanics of walking. *J. Appl. Physiol.* **21**, 271–278. (doi:10.1152/jappl.1966.21.1.271)
4. Wei F, Crechiolo A, Haut RC. 2019 Prediction of ground reaction forces in level and incline/decline walking from a multistage analysis of plantar pressure data. *J. Biomech.* **84**, 46–51. (doi:10.1016/j.jbiomech.2018.12.015)
5. Grundy M, Tosh PA, McLeish RD, Smidt L. 1975 An investigation of the centres of pressure under the foot while walking. *J. Bone Joint Surg. Br.* **57**, 98–103. (doi:10.1302/0301-620X.57B1.98)
6. Croft JL, Bertram JEA. 2020 Form in the context of function: Fundamentals of an energy effective striding walk, the role of the plantigrade foot and its expected size. *Am. J. Phys. Anthropol.* **173**, 760–767. (doi:10.1002/ajpa.24122)
7. Nilsson J, Thorstensson A. 1989 Ground reaction forces at different speeds of human walking and running. *Acta Physiol. Scand.* **136**, 217–227. (doi:10.1111/j.1748-1716.1989.tb08655.x)
8. Jung Y, Jung M, Lee K, Koo S. 2014 Ground reaction force estimation using an insole-type pressure mat and joint kinematics during walking. *J. Biomech.* **47**, 2693–2699. (doi:10.1016/j.jbiomech.2014.05.007)
9. Warabi T, Kato M, Kiriyama K, Yoshida T, Kobayashi N. 2005 Treadmill walking and overground walking of human subjects compared by recording sole–floor reaction force. *Neurosci. Res.* **53**, 343–348. (doi:10.1016/j.neures.2005.08.005)
10. Wang X, Ma Y, Hou BY, Lam WK. 2017 Influence of gait speeds on contact forces of lower limbs. *J. Healthc. Eng.* **2017**, 6375976. (doi:10.1155/2017/6375976). Erratum in: *J. Healthc. Eng.* **2018**, 9291423.
11. Johnston ER, Mazurek DF, Beer FP, Eisenberg ER. 2010 *Vector mechanics for engineers: statics*. Singapore: McGraw-Hill.
12. Pandolf KB, Haisman MF, Goldman RF. 1976 Metabolic energy expenditure and terrain coefficients for walking on snow. *Ergonomics* **19**, 683–690. (doi:10.1080/00140137608931583)
13. McIntosh AS, Beatty KT, Dwan LN, Vickers DR. 2006 Gait dynamics on an inclined walkway. *J. Biomech.* **39**, 2491–2502. (doi:10.1016/j.jbiomech.2005.07.025)
14. Björklund G, Swarén M, Born DP, Stöggl T. 2019 Biomechanical adaptations and performance indicators in short trail running. *Front. Physiol.* **10**, 506. (doi:10.3389/fphys.2019.00506)
15. Lovejoy CO. 2005 The natural history of human gait and posture. Part 1. Spine and pelvis. *Gait Posture* **21**, 95–112. (doi:10.1016/j.gaitpost.2004.01.001)
16. Ruff C. 2017 Mechanical constraints on the hominin pelvis and the 'obstetrical dilemma'. *Anat. Rec. (Hoboken)* **300**, 946–955. (doi:10.1002/ar.23539)
17. Latimer B, Lovejoy CO. 1989 The calcaneus of *Australopithecus afarensis* and its implications for the evolution of bipedality. *Am. J. Phys. Anthropol.* **78**, 369–386. (doi:10.1002/ajpa.1330780306)
18. Morton DJ. 1924 Evolution of the human foot II. *Am. J. Phys. Anthropol.* **7**, 1–52. (doi:10.1002/ajpa.1330070114)
19. McNutt EJ, Zipfel B, DeSilva JM. 2018 The evolution of the human foot. *Evol. Anthropol.* **27**, 197–217. (doi:10.1002/evan.21713)
20. Farris DJ, Kelly LA, Cresswell AG, Lichtwark GA. 2019 The functional importance of human foot muscles for bipedal locomotion. *Proc. Natl Acad. Sci. USA* **116**, 1645–1650. (doi:10.1073/pnas.1812820116)
21. Hatala KG, Wunderlich RE, Dingwall HL, Richmond BG. 2016 Interpreting locomotor biomechanics from the morphology of human footprints. *J. Hum. Evol.* **90**, 38–48. (doi:10.1016/j.jhevol.2015.08.009)
22. Ruff C, Holt B, Trinkaus E. 2006 Who's afraid of the big bad Wolff?: 'Wolff's law' and bone functional adaptation. *Am. J. Phys. Anthropol.* **129**, 484–498. (doi:10.1002/ajpa.20371)
23. Skedros JG, Brand RA. 2011 Biographical sketch: Georg Hermann von Meyer (1815–1892). *Clin. Orthop. Relat. Res.* **469**, 3072–3076. (doi:10.1007/s11999-011-2040-6)
24. Suri C, Shojaei I, Bazrgar B. 2020 Effects of school backpacks on spine biomechanics during daily activities: a narrative review of literature. *Hum. Factors.* **62**, 909–918. (doi:10.1177/0018720819858792)

25. Russell F, Kormushev P, Vaidyanathan R, Ellison P. 2020 The impact of ACL laxity on a bicondylar robotic knee and implications in human joint biomechanics. *IEEE Trans. Biomed. Eng.* **67**, 2817–2827. (doi:10.1109/TBME.2020.2971855)
26. Schmalz T, Schändlinger J, Schuler M, Bornmann J, Schirrmeister B, Kannenberg A, Ernst M. 2019 Biomechanical and metabolic effectiveness of an industrial exoskeleton for overhead work. *Int. J. Environ. Res. Public Health* **16**, 4792. (doi:10.3390/ijerph16234792)
27. Winter DA. 1988 *The biomechanics and motor control of human gait*. Waterloo, Ont.: University of Waterloo Press.
28. Fischer AG, Wolf A. 2016 Body weight unloading modifications on frontal plane joint moments, impulses and center of pressure during overground gait. *Clin. Biomech. (Bristol, Avon)* **39**, 77–83. (doi:10.1016/j.clinbiomech.2016.09.005)
29. Taylor CR. 1985 Force development during sustained locomotion: a determinant of gait, speed and metabolic power. *J. Exp. Biol.* **115**, 253–262. (doi:10.1242/jeb.115.1.253)
30. Wolff J. 2010 The classic: On the inner architecture of bones and its importance for bone growth. *Clin. Orthop. Relat. Res.* **468**, 1056–1065. (doi:10.1007/s11999-010-1239-2)
31. Frost HM. 2004 A 2003 update of bone physiology and Wolff's Law for clinicians. *Angle Orthod.* **74**, 3–15. (https://meridian.allenpress.com/angle-orthodontist/issue/74/1)
32. Kivell TL. 2016 A review of trabecular bone functional adaptation: What have we learned from trabecular analyses in extant hominoids and what can we apply to fossils? *J. Anat.* **228**, 569–594. (doi:10.1111/joa.12446)
33. Currey JD. 2003 The many adaptations of bone. *J. Biomech.* **36**, 1487–1495. (doi:10.1016/s0021-9290(03)00124-6)
34. Schijve J. 2009 *Fatigue of structures and materials*, 2nd edn. Berlin, Germany: Springer Science & Business Media.
35. Folman Y, Wosk J, Voloshin A, Liberty S. 1986 Cyclic impacts on heel strike: a possible biomechanical factor in the etiology of degenerative disease of the human locomotor system. *Arch. Orthop. Trauma Surg.* **104**, 363–365. (doi:10.1007/BF00454431)
36. Lautzenheiser SG, Kramer PA. 2013 Linear and angular measurements of the foot of modern humans: a test of Morton's foot types. *Anat. Rec. (Hoboken)* **296**, 1526–1533. (doi:10.1002/ar.22764)
37. DeSilva JM, Bonne-Annee R, Swanson Z, Gill CM, Sobel M, Uy J, Gill SV. 2015 Midtarsal break variation in modern humans: functional causes, skeletal correlates, and paleontological implications. *Am. J. Phys. Anthropol.* **156**, 543–552. (doi:10.1002/ajpa.22699)
38. Bates KT *et al.* 2013 The evolution of compliance in the human lateral mid-foot. *Proc. R. Soc. B* **280**, 20131818. (doi:10.1098/rspb.2013.1818)
39. De Wit B, De Clercq D, Aerts P. 2000 Biomechanical analysis of the stance phase during barefoot and shod running. *J. Biomech.* **33**, 269–278. (doi:10.1016/s0021-9290(99)00192-x)
40. Divert C, Mornieux G, Freychat P, Baly L, Mayer F, Belli A. 2008 Barefoot-shod running differences: shoe or mass effect? *Int. J. Sports Med.* **29**, 512–518. (doi:10.1055/s-2007-989233)
41. Squadrone R, Gallozzi C. 2009 Biomechanical and physiological comparison of barefoot and two shod conditions in experienced barefoot runners. *J. Sports Med. Phys. Fitness.* **49**, 6–13.
42. Lieberman DE, Venkadesan M, Werbel WA, Daoud AI, D'Andrea S, Davis IS, Mang'eni RO, Pitsiladis Y. 2010 Foot strike patterns and collision forces in habitually barefoot versus shod runners. *Nature* **463**, 531–535. (doi:10.1038/nature08723)
43. Ardigò LP, Lafortuna C, Minetti AE, Mognoni P, Saibene F. 1995 Metabolic and mechanical aspects of foot landing type, forefoot and rearfoot strike, in human running. *Acta Physiol. Scand.* **155**, 17–22. (doi:10.1111/j.1748-1716.1995.tb09943.x)
44. Bobbert MF, Yeadon MR, Nigg BM. 1992 Mechanical analysis of the landing phase in heel–toe running. *J. Biomech.* **25**, 223–234. (doi:10.1016/0021-9290(92)90022-s)
45. Heidner GS, Nascimento RB, Aires AG, Baptista RR. 2020 Barefoot walking changed relative timing during the support phase but not ground reaction forces in children when compared to different footwear conditions. *Gait Posture* **83**, 287–293. (doi:10.1016/j.gaitpost.2020.10.034)
46. Kim HY, Shin HS, Ko JH, Cha YH, Ahn JH, Hwang JY. 2017 Gait analysis of symptomatic flatfoot in children: an observational study. *Clin. Orthop. Surg.* **9**, 363–373. (doi:10.4055/cios.2017.9.3.363)
47. Badhyal S, Dhole SR, Gopinathan NR, Dhillon MS, Dhiman V, Jayal AD, Prasad J. 2019 Kinetic and kinematic analysis of gait in Type IV osteogenesis imperfecta patients: a comparative study. *Indian J. Orthop.* **53**, 560–566. (doi:10.4103/ortho.IJOrtho_291_18)
48. Kramer PA. 2010 The effect on energy expenditure of walking on gradients or carrying burdens. *Am. J. Hum. Biol.* **22**, 497–507. (doi:10.1002/ajhb.21027)
49. Louey MGY, Mudge A, Wojciechowski E, Sangeux M. 2017 A model to calculate the progression of the centre of pressure under the foot during gait analysis. *Gait Posture* **57**, 147–153. (doi:10.1016/j.gaitpost.2017.06.004)
50. Diggle PJ, Gómez-Rubio V, Brown PE, Chetwynd AG, Gooding S. 2007 Second-order analysis of inhomogeneous spatial point processes using case-control data. *Biometrics* **63**, 550–557. (doi:10.1111/j.1541-0420.2006.00683.x)
51. Ben-Hamo M, Ezra D, Krasnov H, Blank L. 2020 Spatial and temporal dynamics of mal secco disease spread in lemon orchards in Israel. *Phytopathology* **110**, 863–872. (doi:10.1094/PHYTO-06-19-0195-R)
52. Elliott P, Wakefield J. 2001 Disease clusters: should they be investigated, and, if so, when and how? *J. R. Stat. Soc. A* **164**, 3–12. (doi:10.1111/1467-985X.00180)
53. Maciel-Nájera JF, Hernández-Velasco J, González-Elizondo MS, Hernández-Díaz JC, López-Sánchez CA, Antúnez P, Bailón-Soto CE, Wehenkel C. 2020 Unexpected spatial patterns of natural regeneration in typical uneven-aged mixed pine–oak forests in the Sierra Madre Occidental, Mexico. *Global Ecol. Conserv.* **23**, e01074. (doi:10.1016/j.gecco.2020.e01074)
54. Lisitsin V. 2015 Spatial data analysis of mineral deposit point patterns: applications to exploration targeting. *Ore Geol. Rev.* **71**, 861–881. (doi:10.1016/j.oregeorev.2015.05.019)
55. Jafari-Mamaghani M, Andersson M, Krieger P. 2010 Spatial point pattern analysis of neurons using Ripley's *K*-function in 3D. *Front. Neuroinform.* **4**, 9. (doi:10.3389/fninf.2010.00009)
56. Ge W, Wang L, Sun Y, Liu X. 2019 An efficient method to generate random distribution of fibers in continuous fiber reinforced composites. *Polym. Compos.* **40**, 4763–4770. (doi:10.1002/pc.25344)
57. Tianbo C, Sun Y, Maadooliat M. 2020 Collective spectral density estimation and clustering for spatially-correlated data. *Spatial Statist.* **38**, 100451. (doi:10.1016/j.spasta.2020.100451)
58. Zhou Y, Lau BPL, Koh Z, Yuen C, Ng BKK. 2020 Understanding crowd behaviors in a social event by passive wifi sensing and data mining. *IEEE Internet Things J.* **7**, 4442–4454. (doi:10.1109/JIOT.2020.2972062)
59. Cao R, Li B, Wang Z, Peng ZR, Tao S, Lou S. 2020 Using a distributed air sensor network to investigate the spatiotemporal patterns of PM2.5 concentrations. *Environ. Pollut.* **264**, 114549. (doi:10.1016/j.envpol.2020.114549)
60. Zia A *et al.* 2020 Characterizing heterogeneous behavior of non-point-source polluters in a spatial game under alternate sensing and incentive designs. *J. Water Resour. Plann. Managem.* **146**, 13pp. (doi:10.1061/(ASCE)WR.1943-5452.0001242)
61. Ahmadi R, Shahrabi J, Aminshahidy B. 2020 Forcasting multiple-well flow rates using a novel space–time modeling approach. *J. Petroleum Sci. Eng.* **191**, 107027. (doi:10.1016/j.petrol.2020.107027)
62. Hofmann UK, Götze M, Wiesenreiter K, Müller O, Wünschel M, Mittag F. 2019 Transfer of plantar pressure from the medial to the central forefoot in patients with hallux valgus. *BMC Musculoskelet. Disord.* **20**, 149. (doi:10.1186/s12891-019-2531-2)
63. Pataky TC. 2012 Spatial resolution in plantar pressure measurement revisited. *J. Biomech.* **45**, 2116–2124. (doi:10.1016/j.jbiomech.2012.05.038)
64. Maurer JD, Ward V, Mayson TA, Davies KR, Alvarez CM, Beauchamp RD, Black AH. 2014 Classification of midfoot break using multi-segment foot kinematics and pedobarography. *Gait Posture* **39**, 1–6. (doi:10.1016/j.gaitpost.2013.08.015)
65. Bosch K, Nagel A, Weigend L, Rosenbaum D. 2009 From 'first' to 'last' steps in life—pressure patterns of three generations. *Clin. Biomech. (Bristol, Avon)* **24**, 676–681. (doi:10.1016/j.clinbiomech.2009.06.001)

66. Booth BG, Keijsers NLW, Sijbers J, Huysmans T. 2018 STAPP: spatiotemporal analysis of plantar pressure measurements using statistical parametric mapping. *Gait Posture* **63**, 268–275. (doi:10.1016/j.gaitpost.2018.04.029)
67. Hughes J, Clark P, Jagoe RR, Gerber C, Klenerman L. 1991 The pattern of pressure distribution under the weightbearing forefoot. *The Foot.* **1**, 117–124. (doi:10.1016/0958-2592(91)90020-C)
68. Ripley B. 1976 The second-order analysis of stationary point processes. *J. Appl. Probab.* **13**, 255–266. (doi:10.2307/3212829)
69. Ripley BD. 1991 *Statistical inference for spatial processes*. Cambridge, UK: Cambridge University Press.
70. Cavanagh PR, Rodgers MM. 1987 The arch index: a useful measure from footprints. *J. Biomech.* **20**, 547–551. (doi:10.1016/0021-9290(87)90255-7)
71. Stöggl T, Martiner A. 2017 Validation of Moticon's OpenGo sensor insoles during gait, jumps, balance and cross-country skiing specific imitation movements. *J. Sports Sci.* **35**, 196–206. (doi:10.1080/02640414.2016.1161205)
72. Baddeley A, Turner R, Rubak E. 2015 *Spatial point patterns: methodology and applications with R*. London, UK: CRC Press.
73. Sarkar D. 2008 *Lattice: multivariate data visualization with R*. New York, NY: Springer.
74. Pebesma EJ, Bivand RS. 2005 Classes and methods for spatial data in R, vol. 5. *R News*. See https://cran.r-project.org/doc/Rnews/.
75. Rowlingson B, Diggle P. 2017 *Splancs: spatial and space–time point pattern analysis*. R package version 2.01-40. See https://CRAN.R-project.org/package=splancs
76. Bates D, Maechler M, Bolker B, Walker S. 2015 Fitting linear mixed-effects models using lme4. *J. Stat. Softw.* **67**, 1–48. (doi:10.18637/jss.v067.i01)
77. Emerson SS, Spieker AJ, Williamson BD, Hee Wai TY, Lim S. 2018 *uwIntroStats: descriptive statistics, inference, regression, and plotting in an introductory statistics course*. R package version 0.0.7. See https://CRAN.R-project.org/package=uwIntroStats.
78. Hennig EM, Staats A, Rosenbaum D. 1994 Plantar pressure distribution patterns of young school children in comparison to adults. *Foot Ankle Int.* **15**, 35–40. (doi:10.1177/107110079401500107)
79. Rosenbaum D. 2013 Foot loading patterns can be changed by deliberately walking with in-toeing or out-toeing gait modifications. *Gait Posture* **38**, 1067–1069. (doi:10.1016/j.gaitpost.2013.04.001)
80. McKay MJ, Baldwin JN, Ferreira P, Simic M, Vanicek N, Wojciechowski E, Mudge A, Burns J. (for the 1000 Norms Project 2017 Consortium). 2017 Spatiotemporal and plantar pressure patterns of 1000 healthy individuals aged 3–101 years. *Gait Posture* **58**, 78–87. (doi:10.1016/j.gaitpost.2017.07.004)
81. Jameson EG, Davids JR, Anderson JP, Davis 3rd RB, Blackhurst DW, Christopher LM. 2008 Dynamic pedobarography for children: use of the center of pressure progression. *J. Pediatr. Orthop.* **28**, 254–258. (doi:10.1097/BPO.0b013e318164ee6e)
82. Blackburn JT, Pietrosimone BG, Harkey MS, Luc BA, Pamukoff DN. 2016 Comparison of three methods for identifying the heelstrike transient during walking gait. *Med. Eng. Phys.* **38**, 581–585. (doi:10.1016/j.medengphy.2016.04.008)
83. Whittle MW. 1999 Generation and attenuation of transient impulsive forces beneath the foot: a review. *Gait Posture.* **10**, 264–275. (doi:10.1016/s0966-6362(99)00041-7)
84. Takahashi KZ, Gross MT, van Werkhoven H, Piazza SJ, Sawicki GS. 2016 Adding stiffness to the foot modulates soleus force–velocity behaviour during human walking. *Sci. Rep.* **6**, 29870. (doi:10.1038/srep29870)
85. Holowka NB, Lieberman DE. 2018 Rethinking the evolution of the human foot: insights from experimental research. *J. Exp. Biol.* **221**, jeb174425. (doi:10.1242/jeb.174425)
86. Lovejoy CO, Latimer B, Suwa G, Asfaw B, White TD. 2009 Combining prehension and propulsion: the foot of *Ardipithecus ramidus*. *Science* **326**, 72e1-8. (doi:10.1126/science.1175832)
87. Perry J, Boyd LA, Rao SS, Mulroy SJ. 1997 Prosthetic weight acceptance mechanics in transtibial amputees wearing the Single Axis, Seattle Lite, and Flex Foot. *IEEE Trans. Rehabil. Eng.* **5**, 283–289. (doi:10.1109/86.650279)
88. Halsne EG, Czerniecki JM, Shofer JB, Morgenroth DC. 2020 The effect of prosthetic foot stiffness on foot–ankle biomechanics and relative foot stiffness perception in people with transtibial amputation. *Clin. Biomech. (Bristol, Avon)* **80**, 105141. (doi:10.1016/j.clinbiomech.2020.105141)
89. Rábago CA, Wilken JM. 2016 The prevalence of gait deviations in individuals with transtibial amputation. *Mil. Med.* **181**(S4), 30–37. (doi:10.7205/MILMED-D-15-00505)
90. Pew CA, Roelker SA, Klute GK, Neptune RR. 2020 Analysis of the relative motion between the socket and residual limb in transtibial amputees while wearing a transverse rotation adapter. *J. Appl. Biomech.* **37**, 21–29. (doi:10.1123/jab.2019-0362)
91. Kim M, Lyness H, Chen T, Collins S. 2020 Prosthesis inversion/eversion stiffness reduces balance-related variability during level walking. *J. Biomech. Eng.* **142**, 091011. (doi:10.1115/1.4046881)
92. Fey NP, Klute GK, Neptune RR. 2011 The influence of energy storage and return foot stiffness on walking mechanics and muscle activity in below-knee amputees. *Clin. Biomech. (Bristol, Avon)* **26**, 1025–1032. (doi:10.1016/j.clinbiomech.2011.06.007)
93. Timmermans C, Cutti AG, van Donkersgoed H, Roerdink M. 2019 Gaitography on lower-limb amputees: repeatability and between-methods agreement. *Prosthet. Orthot. Int.* **43**, 71–79. (doi:10.1177/0309364618791618)
94. Serrancolí G, Kinney AL, Fregly BJ. 2020 Influence of musculoskeletal model parameter values on prediction of accurate knee contact forces during walking. *Med. Eng. Phys.* **85**, 35–47. (doi:10.1016/j.medengphy.2020.09.004)
95. Charles JP, Fu FH, Anderst W. 2020 Predictions of anterior cruciate ligament dynamics from subject-specific musculoskeletal models and dynamic biplane radiography. *J. Biomech. Eng.* **143**, 031006. (doi:10.1115/1.4048710)
96. Kram R, Taylor CR. 1990 Energetics of running: a new perspective. *Nature* **346**, 265–267. (doi:10.1038/346265a0)
97. Hammerberg AG, Kramer PA. 2021 Data from: Consistent inconsistencies in braking: a spatial analysis. Figshare.